Boreal canopy surfaces from spaceborne stereogrammetry

Paul M. Montesano[a,b], Christopher S.R. Neigh[b], William Wagner[a,b], Margaret Wooten[a,b], Bruce D. Cook[b]

Affiliations

a Science Systems and Applications, Inc., 10210 Greenbelt Road, Lanham, MD 20706, USA

b Code 618, Biospheric Sciences Laboratory, NASA Goddard Space Flight Center, Greenbelt MD 20771

Keywords: forest structure; boreal; stereogrammetry; photogrammetry; digital surface model; canopy height

Abstract

Surface elevation estimates from high resolution spaceborne image (HRSI) stereogrammetry are used to examine fine-scaled structure of boreal forest canopies. These data can depict detailed spatial patterns of vertical forest structure at remote sites across the circumpolar domain where these estimates would otherwise be unavailable. This work examines where these estimates are most effective at describing vertical forest structure to explain which canopy surfaces they represent. We evaluated the variation in canopy surface estimates captured from four general types of HRSI digital surface models (DSMs) across the full range of boreal canopy cover. These DSMs, classified into 4 types by grouping them according to the acquisition's (1) sun elevation angle (low or high) and (2) seasonality-driven ground surface condition (snow presence/absence), vary with acquisition characteristics and the details of this variation continues to be studied. We explored some of this variation by comparing the distributions of differences in boreal canopy percentile heights derived from reference small footprint lidar in Tanana Valley, Alaska with canopy surface elevations derived from these 4 types of HRSI DSMs. We examined how canopy surface estimates from HRSI DSMs differ according to acquisition characteristics and canopy cover, and ultimately which canopy surfaces are represented in these DSMs. Our results help clarify which boreal canopy surfaces are representative of those captured with HRSI DSMs. They show

that in the Tanana Valley (1) DSMs grouped by sun elevation angle and ground surface condition provide different surface estimates of boreal canopies; (2) the two DSM types that appear to most differently capture boreal forest canopy surfaces are DSMs from snow-free images acquired at sun elevation angles < 30° (Low sun elev. & snow-free) and those with snow-cover at sun elevation angles ≥ 30° (High sun elev. & snow-free); (3) DSMs with snow most often do not capture upper canopy surfaces; (4) the “Low sun elev. & snow-free” DSMs resolve surfaces that are most representative of upper canopy surfaces (dense forests > 60% cover, 70th - 80th percentile heights); and (5) in the most dense forests (> 80% cover) where canopy gaps are least likely to bias downward the average surface estimates, the snow-free DSM types are representative of 70th - 80th percentile heights (“Low sun elev. & snow-free”) and 60th - 70th percentile heights (“High sun elev. & snow-free”). The combination of horizontal structure (canopy cover) and acquisition characteristics affect the boreal vertical structure (canopy surface height) estimates from spaceborne stereogrammetry. These effects should be considered when analyzing products derived from HRSI DSMs, and as part of a comprehensive approach to spaceborne remote sensing of circumpolar boreal forests.

Introduction

Fine-scaled forest structure estimates reveal important variation in the structural patterns of groups of trees that help regulate ecosystem dynamics in the high-latitudes (> 60° N). Near the northern limit of trees, their spatial pattern may be a feature that helps explain changes at the forest tundra ecotone (Harper et al., 2011). The aboveground biomass associated with these forests may constitute a relatively small component of overall carbon stocks, but such structural attributes may be linked to thaw depth and belowground carbon storage (Pan et al., 2011; Webb et al., 2017). Patterns of forest structure indicate successional stages, revealing carbon accumulation characteristics in larch recovering from disturbances (Alexander et al., 2012; Siewert et al., 2015). The structure of boreal forests, composed of horizontal (eg., canopy cover) and vertical (eg., canopy surface height) characteristics, are required input to initialize, update, and test predictions from ecosystem models that, particularly in high-latitudes, may uncover key processes associated with the climate-vegetation interactions (Forkel et al., 2016; Hurtt et al., 2016; Shugart et al., 2010; Snyder and Liess, 2013; Wang et al., 2016).

Recent work has shown that three-dimensional (e.g., stereogrammetric) analysis of fine-scaled spaceborne remote sensing data (i.e., high resolution spaceborne imagery; HRSI), or its airborne counterpart, can provide detailed estimates of vertical forest structure (St-Onge et al. 2008, Bohlin et al., 2012; Hawryło et al., 2017; Kattenborn et al., 2015; Montesano et al., 2017; Neigh et al., 2014; Puliti et al., 2016; Vastaranta et al., 2014; Persson and Perko, 2016; Fassnacht et al., 2017; Immitzer et al., 2016). However, important challenges remain that are associated with deriving these estimates at relevant spatial scales from optical images. In particular, challenges arise from variations in the solar geometry of an image acquisition, whereby this variation may affect estimates of forest structure through the increased uncertainty of canopy surface height estimates. Shadows in images, and the associated decrease in contrast, results in higher errors in elevation from stereogrammetric surface estimates (Honkavaara et al., 2012). These shadows are more extensive at low sun elevation angles and in areas of greater terrain relief. Low sun angles, however, can be a useful acquisition feature to exploit for capturing heights of groups of trees in sparse forests (Montesano et al., 2017).

Sensor geometry can also affect the ability to capture forest structure. Broad differences in the view angles of each image of a stereopair will limit the success of automated stereogrammetry routines as correlation algorithms fail to find matching points between two images acquired from sufficiently different viewing directions (Hobi et al., 2015; Wulder et al., 2008). Some studies report acquisition parameters for the data in their study, which may provide some understanding of how stereopairs may capture forest surfaces (Straub et al., 2013). However, such sun-sensor-target acquisition geometry information is not yet routinely linked to forest structure estimates.

The uncertainty of stereogrammetric estimates of forest surfaces may also depend on the forest structure itself. The vertical structure of sparse forests can be quantified with different types of DSMs based on sun elevation angle because forest gaps are relatively large, and ground surface estimates are possible (Montesano et al., 2017). However, in denser forest, estimates from airborne stereogrammetry do not resolve gaps well (White et al., 2018), and this limitation is exacerbated with stereopairs acquired at low sun elevation angles. White et al (2018) suggest that occlusion and shadows limit detection of gaps with digital aerial photogrammetric estimates. Poor gap detection will result in overestimates of boreal forest canopy cover and volume and thus some structural attributes derived from stereogrammetry are more reliably captured (e.g., stand dominant height) than others (e.g., growing stock volume) (Järnstedt et al., 2012).

The effects of HRSI acquisition characteristics on forest structure estimates can be pronounced in high latitudes. In these regions, the short growing season features longer diurnal periods that enable acquisitions across a broad range of sun elevation angles. As such, remote sensing with HRSI in high latitude forests offers unique opportunities to examine the variability of structure estimates from these data. These forests are sometimes comprised of open canopies where the ground is visible between individual crowns, but this pattern of tree cover can vary widely. What may appear as open canopy forest in terms of overall percent canopy cover at coarse scales (e.g., hundreds of meters) may manifest as a few dense clusters of near continuous tree cover in an area otherwise devoid of forest. These differences in forest structure appear as differences in images texture in HRSI (Beguet et al., 2014; Moskal and Franklin, 2002).

Differences in forest structure need to be consistently captured across space to accurately describe its pattern. This consistency is needed from products derived from a mosaic of individual DSMs with different acquisition characteristics. The ArcticDEM is a land surface elevation product derived from HRSI DSMs for the areas primarily above 60°N (Morin et al., 2016, http://arcticdem.org). This product, posted at 2m spatial resolution, features stereogrammetric surface elevation estimates above a reference ellipsoid compiled from along-track stereopair acquisitions of sub-meter panchromatic imagery from sensors in the DigitalGlobe constellation (https://www.digitalglobe.com/about/our-constellation). These data feature systematic vertical and horizontal offsets of generally around 3 - 5 m, and have a vertical uncertainty of ~ 0.2 m after co-registration (Noh and Howat, 2015; Shean et al., 2016). The along-track stereopairs are collected as strips ~ 17 km in the east-west direction, and ~ 110 km north-south. The

ArcticDEM is a compilation of these strips acquired across a broad range of sun and sensor acquisition characteristics, and ground conditions throughout all seasons. This dataset is being used in hydrologic and forest structure studies (Dai et al., 2018; Dai and Howat, 2017; Meddens et al. 2018). The ArcticDEM has forest canopy surface estimates included in the DEM product (Meddens et al. 2018). Extracting that signal may require some prior knowledge of acquisition characteristics and forest structure. Because of the challenges that arise from the variation in acquisition characteristics, the interpretation of estimates of forest structure from HRSI DSMs may benefit from a general understanding of the forest structure in question and the parameters of HRSI acquisitions. This may inform the uncertainty of DSM-derived structure estimates, and serve as general purpose spatial masks for understanding where estimates are most useful for explaining forest structure.

Despite challenges to the use of HRSI for forest structure estimates, there is significant potential for using derived forest structure estimates for forest growth modelling and assessments of current carbon patterns and fluxes. For example, HRSI may be used to improve continuous maps of above-ground biomass density (AGB) derived from discontinuous estimates of AGB from lidar sampling. These data can potentially be useful for filling in gaps in lidar coverage used for spatially detailed estimates of AGB across broad scales. Additionally, these data may have value as potential supplements to existing forest inventory plot and lidar data. The often sparse inventory data form the basis of modelling frameworks that, when linked to forest structure derived from small footprint lidar, are used to predict AGB across broad extents. These models can be improved with more forest structure information that can be used either in cross-validation of modelled estimates of forest structure or for providing estimates where lidar is absent, resulting in better model predictions of forest structure and its uncertainty (Babcock et al., 2018, 2015; Finley et al., 2017; Saarela et al. 2016; Puliti et al. 2018).

The objective of this work is to examine spaceborne DSM estimates of the vertical component of boreal forest structure, the canopy surfaces. We examine these DSMs by grouping them according to type, a combination of the solar elevation angle and the ground surface condition (snow presence or absence) at the time of image acquisition. Our focus is to (1) assess which canopy surfaces within the vertical forest structure column are most representative of those canopy surfaces from the various DSM types, and (2) examine how the canopy surfaces from these DSM estimates vary with forest canopy cover and acquisition characteristics.

Methods

Overview

To address the objective of this work we chose study sites in the Tanana Inventory Unit (TIU) across the Tanana Valley, Alaska, situated north and east of the Alaska Range. At these sites, small-footprint airborne lidar and spaceborne DSMs provide recent (2012 – 2016) estimates of a range of horizontal and vertical boreal forest structure (Figure 1a). The TIU is a part of interior Alaska where it's boreal (taiga) forests experience a continental climate and are composed primarily of species belonging to the genus' Picea, Larix, Betula or Populus (Stuart Chapin et al., 2006). The mosaic of forest structure patterns (in terms of forest canopy cover, density, age, height, vertical distribution of canopy components, etc.) in the TIU reflect the strong role that fire disturbance continues to have in the region, and provides an opportunity to examine with HRSI a wide range of structural conditions. Here, examples of common forest structure patterns feature trees arranged in sparse clusters, dense continuous canopies, standing dead individual trees, and variable mosaics, all of which are linked to the complex interaction between current site conditions and histories (Figure 1b). These forest structure patterns produce distinct textures in HRSI and their associated DSMs.

For this study, we considered spatially coincident comparisons of reference lidar and HRSI DSMs that provided forest structure samples across the full range of canopy cover. We describe (1) the reference canopy structure estimates from airborne lidar, (2) the spaceborne canopy surface estimates derived from stereogrammetry applied to HRSI stereopairs, and the grouping of these DSMs by acquisition conditions, (3) the process of co-registering the reference airborne lidar digital terrain models (DTMs) with the spaceborne DSMs, and (4) the process of compiling a database of differences between DSMs and reference surfaces used in the analysis.

a

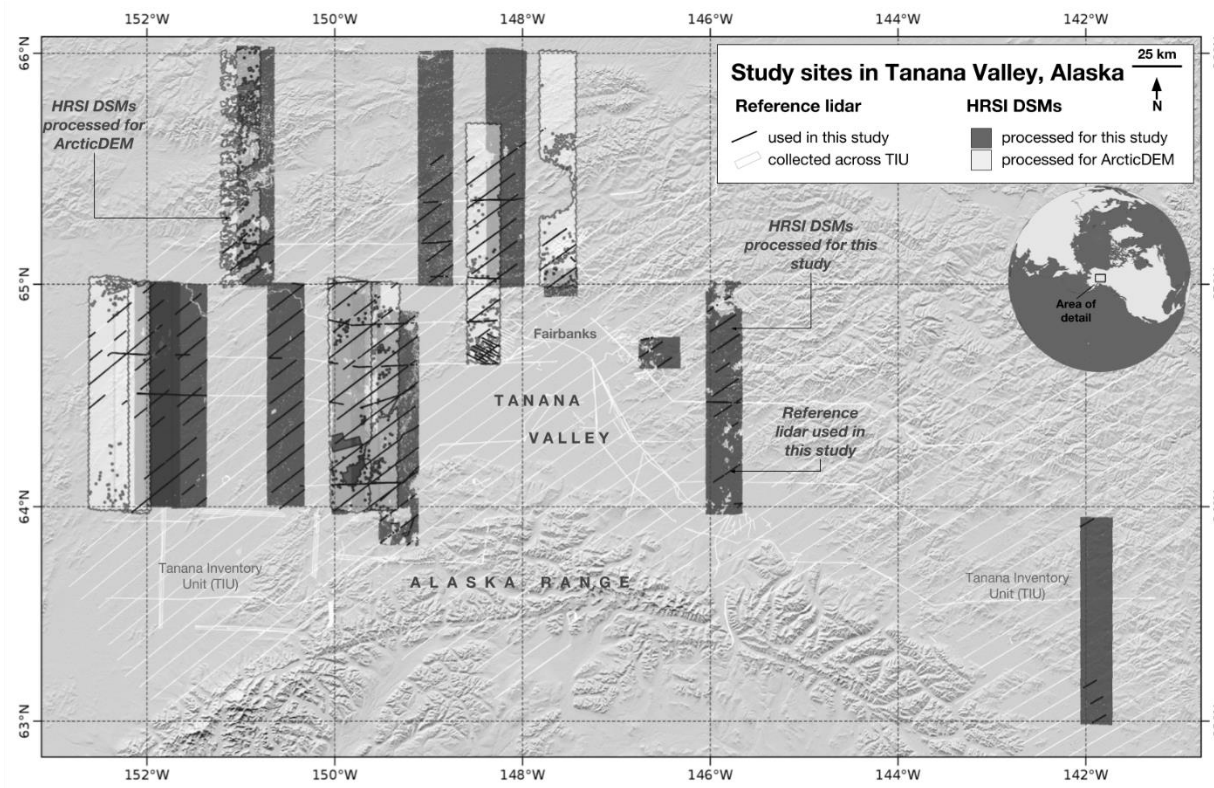

b

Figure 1. (a) Study sites in the Tanana Valley, Alaska where reference lidar provided reference measurements of horizontal and vertical forest structure for coincident strips of HRSI DSMs. (b) Aerial images of acquired during the 2014 airborne survey of the TIU with a digital single-lens reflex camera highlight a variety of forest structure patterns including (from left to right) small groups of conifers, dense continuous canopy, dense canopy adjacent to standing dead and fallen trees, and heterogeneous canopy cover.

Reference canopy surfaces from lidar

The reference canopy surfaces from lidar provided estimates of canopy structure (height and cover) against which DSM canopy surfaces were compared. They were derived from small-footprint airborne lidar acquired by NASA Goddard's Lidar, Hyperspectral and Thermal Imager (GLiHT; (Cook et al., 2013); (Corp et al., 2015)) in the Tanana Valley in July - August 2014. These data were collected with a strip-sampling approach along flightlines primarily oriented NE-SW, nominally 335 m above ground, a footprint of ~ 10 cm in diameter, and a pulse density of ~ 4 m^{-2} with up to 8 lidar returns per pulse, such that there was a maximum of 32 returns m^{-2}. However, for the forest structure captured in this dataset ~ 2-3 returns per pulse is more typical, resulting in an expected lidar return density of ~ 8-12 returns m^{-2}. The strip-sampling was carried out as swaths ~ 250 m wide spaced at intervals ~ 9.3 km and were designed specifically to capture and quantify the full range of horizontal and vertical forest structure and AGB across the region.

The canopy height estimates describe the vertical structure of TIU forests. They are composed of 10 percentile heights (p10 – p100, in 10% increments) representing a variety of canopy surfaces throughout the vertical canopy column. These surfaces, in meters above the lidar-derived digital terrain model (DTM), describe the height below which the proportion of all lidar canopy returns (i.e., returns classified as 'tree') within a pixel are found for a stated percentile increment. For these data, those returns > 1.37 m above the DTM were classified as 'tree', and the percentile heights were calculated for pixels at 13 m resolution. This pixel size has an area equal to that of coincident US Forest Inventory Assessment (FIA) subplots, and was not chosen specifically for this study. The p100 surface represents the height estimate of the upper-most canopy surface, below which 100% of the 'tree' returns were recorded, while the p10 is the canopy surface below which 10% of the 'tree' returns were recorded, and represented the canopy surface closest to the ground.

The canopy cover estimates describe the horizontal structure of TIU forests. These estimates describe the proportion of all returns that are classified as 'tree' on a per-pixel basis. This horizontal structure provides important reference for understanding for examining how the vertical structure is captured in the HRSI DSMs, because it provides an estimate of canopy density. The density of the canopy effects the apparent roughness of the canopy surfaces as seen in the HRSI data. Figure 2 summarizes forest structure measurements from reference lidar that coincide with HRSI DSMs used in this study. The distribution of reference heights are shown according to 20 % bin canopy cover intervals for 4 of the reference canopy surfaces across the TIU study domain. These reference lidar data provide some context for the structure of forests within the TIU study domain, where the distribution of canopy heights are very different depending on the canopy cover.

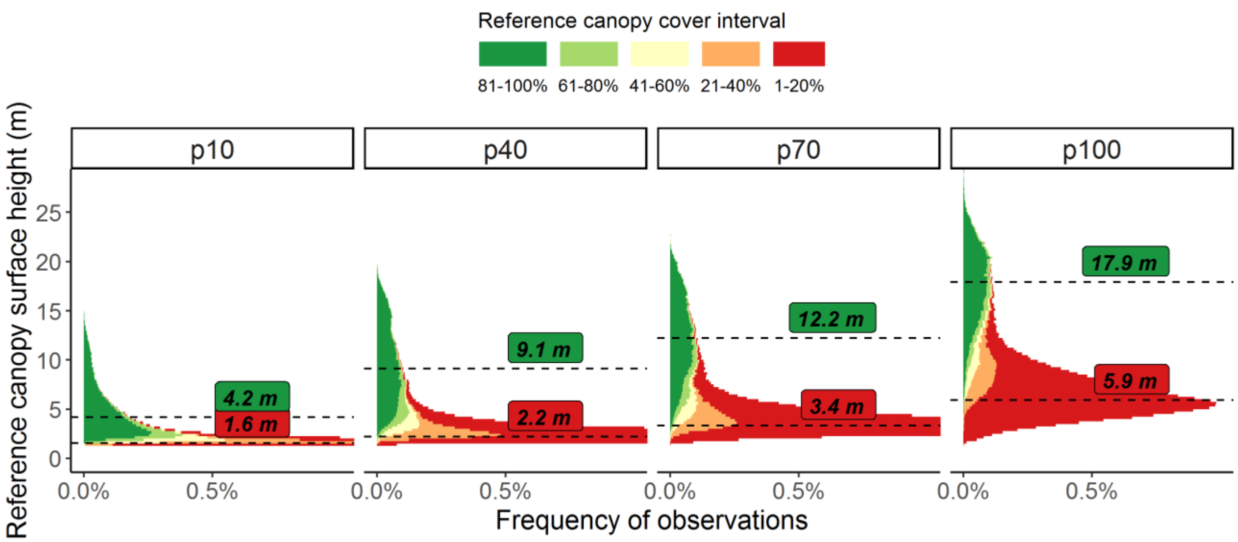

Figure 2. Forest structure across the TIU study domain from reference lidar. The distributions of all reference canopy surface heights for 4 of the 10 percentile heights colored by canopy cover interval across the TIU study domain. Dashed lines and values in colored boxes show the median height values in meters for the corresponding canopy cover intervals.

Spaceborne canopy surfaces from stereogrammetry

The spaceborne DSM canopy estimates used in this study were derived from two similar HRSI stereogrammetry sources and grouped according to acquisition characteristics. These 2 sources provided data that extended the seasonal domain of this study from winter through summer. Each DSM was derived from Level 1B images acquired from DigitalGlobe’s Worldview 1, 2 or 3 satellites. DigitalGlobe provides these data at no-direct cost to U.S. Government agencies and non-profit organizations that support U.S. interests via the NextView license agreement (Neigh et al., 2013). The spatial resolution of these data depend on each acquisition's degree of off-nadir pointing. The typical ranges of resolutions for Worldview-1-2 data span 0.5 m - 0.7 m while that of Worldview-3 spans 0.3 m - 0.55 m. The panchromatic data from each satellite that is used to derive DSMs have an 11 bit dynamic range, and span the spectral ranges 400 nm – 900 nm (Worldview-1) and 450-800 nm (Worldview-2, 3).

The first source of DSM's were those derived from snow-free HRSI that were selected and processed for this study. We selected along-track HRSI stereopairs that matched metadata searches within the TIU geographic coverage to identify primarily 1° HRSI "strips" (each ~17 km × 110 km) with < 50% cloud-cover from months June - September from 2012 - 2016. These DSM were processed with Ames Stereo Pipeline (ASP) v. 2.5.1 using a workflow similar to that described in Shean et al. 2016, with algorithms and parameters described in Montesano et al. 2017, on the NASA Center for Climate Simulation's Advanced Data Analytics Platform at Goddard Space Flight Center (ADAPT, https://www.nccs.nasa.gov/services/adapt) (Montesano et al., 2017; Shean et al., 2016). The routines in ASP form a suite of automated tools for stereogrammetry designed to process spaceborne and airborne stereo imagery. This processing yielded 12 DSMs at 1 m resolution derived from snow-free acquisitions that were used in the analysis.

The second source of DSMs used in this study was that of the ArcticDEM v2 (release 3), a digital surface model of the Arctic derived from stereo HRSI and open source stereogrammetry software (Porter el a. 2018). These data were processing using the Surface Extraction from TIN-based Searchspace Minimization (SETSM) software (Noh and Howat, 2017, 2015) and are provided as 2 m resolution 1° strips, which were the basis for the larger ArcticDEM mosaic. These DSMs were selected from the set of those previously processed across the TIU based on the timing and sun elevation angle of each acquisition. These data spanned both winter and early spring across a range of sun elevation angles, and provided 8 DSMs at 2 m resolution derived from acquisitions all with snow present.

The DigitalGlobe archive offers image stereopairs that have been collected with a range of acquisition characteristics associated with sun and sensor position and ground surface condition. These characteristics may affect the canopy surface estimates of the derived DSMs. We grouped the DSMs used in the canopy surface analysis into 2 categories according to the acquisitions sun elevation angle and 2 categories according to general ground surface condition. DSMs collected at sun elevation angles < 30° were classified as 'Low sun elev.' and those ≥ 30 degrees as 'High sun elev.' DSMs from images that featured snow present across the majority of the ground surface were assigned a condition of 'snow', while those with little or no snow cover were assigned a condition of 'snow-free'. DSMs were grouped according to their classification in each of these categories, creating 4 DSM types. The DSM type was linked to each pixel in the database of pixel-level height values described above.

Co-registration of HRSI DSMs to reference lidar

HRSI DSMs generally feature horizontal and vertical errors < 5 m (DigitalGlobe, 2014). To compare canopy surfaces of these DSMs to those from reference lidar, we co-registered DSMs to lidar by first separating DSM into ground and canopy surfaces. The ground surfaces served as the basis for the co-registration because we assume that ground surfaces serve as static control that did not change between reference lidar and spaceborne DSM acquisitions, and because the differences between the canopy surfaces in these two datasets are the focus of this work. The co-registration portion of the analysis involved (1) identifying a mask of DSM ground surfaces and (2) using this mask to align the ground surfaces of these DSMs with those of the reference DTM, and (3) removing outliers, to compile the initial set of observations whose co-registration seemed sufficient to proceed with further canopy surface analysis.

We identified HRSI DSM ground surfaces by applying a spatial mask of tree canopy cover derived from reference lidar fractional tree cover estimates. This mask excluded all portions of each DSM that corresponded to canopy cover > 0.05 %. The remaining areas, the ground mask, where those where pixels from the HRSI DSMs corresponded to those for which reference lidar indicated a near ground surface.

Within this ground mask, we aligned DSM ground surfaces to those of the reference DTM. First, we calculated offsets between the DSM and the reference DTM, using an iterative closest point algorithm (point-to-point) in the ‘pc_align’ routine from Ames Stereo Pipeline. These offsets accounted for both horizontal and vertical differences between the DSMs and the reference. We then applied a translation based on these offsets to all DSM pixels, yielding a co-registered DSM.

To remove outliers, the co-registered near-ground surfaces of the given HRSI DSM were differenced from the corresponding reference DTM. We removed pixels with differences > 3 m, a conservative threshold that accounted for portions of HRSI DSMs in which shadows may have reduced contrast between adjacent pixels and for which the automated stereogrammetry routine may have returned poor surface elevations estimates. The distribution of the differences from reference for each HRSI DSM was examined to arrive at a final set of DSMs whose mean difference from reference was within +/- 1 m. These steps increased the likelihood that the ground control surfaces were sufficiently aligned between the reference and HRSI DSM data such that we had confidence in subsequent analyses of canopy surface revealing actual differences between the coincident estimates of canopy surfaces instead of those differences being an artifact of initial misregistration.

Compiling a database of DSM canopy surface differences

We compiled a database of DSM canopy surface differences from reference. First, we aggregated DSMs surface estimates to the 13 m spatial resolution of the reference lidar, then we converted each DSM surface estimate to a height above a DTM, and linked each estimate to canopy cover and DSM type information. To convert DSM surfaces to heights above a DTM, we subtracted the ground surface elevation of the reference DTM from the DSM. This step created preliminary canopy surface height estimates (above the reference DTM) in forest patches where the canopy surfaces were derived exclusively from HRSI DSMs. We then applied a secondary alignment step, to shift these preliminary

DSM canopy surface heights, based on a gaussian analysis of the minimum peak of their distribution (Montesano et al. 2017). We applied a 1 pixel buffer to remove forest patch edge pixels and then calculated the difference of each DSM canopy surface height from the set of 10 corresponding reference lidar percentile height estimates. To each of DSM canopy surface height, we assigned 2 canopy cover estimates; one from reference lidar and one from a recent Landsat tree canopy cover product (Sexton et al., 2013; Montesano et al., 2016).

These steps resulted in a database of canopy surface height difference observations (from reference lidar percentile heights) for each pixel (a 13 m resolution aggregation of the original 1 m and 2 m DSM pixels). Each observation was essentially a stack of 10 difference values, corresponding to each of the 10 reference percentile height surface (where each difference value maintained a link to the nominal percentile height from which it was derived), and 2 percent canopy cover values that were then grouped according to the DSM type. Finally, we reduced this database by extracting for each pixel (1) the reference value among each of the 10 percentile heights that minimized the difference to the DSMs canopy height estimate and (2) the name of the percentile height associated with that minimum difference. For each observation, this reduction resulted in the minimum difference value from the set of DSM differences from reference percentile heights. These served as the representative canopy surface estimates from the HRSI DSMs.

Results

The HRSI DSMs co-registered to within +/- 1 m mean vertical difference of the static control ground surfaces of the reference lidar DTMs in the TIU provided the set of observations used in this analysis. These 20 DSMs provided 565,921 observations of DSM canopy surface heights above reference DTM surfaces that were used in the comparison of DSM and reference lidar canopy surfaces. For each DSM, Table 1 summarizes the type, sensor, acquisition date, tallies the number of observations for each canopy cover interval, and the total number across all intervals. The differences of these DSM canopy surface height observations from reference surfaces were compiled into distributions discussed below.

Table 1. List of HRSI DSMs from which observations of canopy surfaces were compared with those from reference lidar in the TIU. The number of observations are summarized by canopy cover interval, and the total is tallied for each DSM.

DSM type	Sensor	Acquisition date (m/d/yyyy)	# of DSM Observations per reference canopy cover interval (%)					Total # of observations per DSM
			1 - 20	21 - 40	41 - 60	61 - 80	81 - 100	
High sun elev. & snow	WV-1	4/10/2013	959	98	809	156	1,010	3,032
	WV-1	4/16/2013	71,314	3,744	2,444	3,490	12,604	93,596
	WV-2	4/6/2016	17,468	5,136	924	2,902	3,438	29,868
High sun elev. & snow-free	WV-2	7/21/2015	27,020	4,542	2,910	3,878	6,662	45,012
	WV-1	8/15/2012	31,180	1,974	1,313	1,205	2,717	38,389
	WV-1	8/8/2014	22,189	1,364	441	492	12,535	37,021
	WV-1	6/17/2016	24,065	1,885	554	634	4,846	31,984
	WV-2	5/22/2015	3,317	197	103	112	639	4,368
	WV-2	6/23/2016	13,116	1,709	909	1,206	2,781	19,721
	WV-3	6/18/2016	7,978	217	115	59	38	8,407
Low sun elev. & snow	WV-1	3/31/2015	29,453	1,909	181	137	1,673	33,353
	WV-1	4/15/2016	12,558	2,325	592	329	857	16,661
	WV-2	1/28/2013	28,736	3,502	1,456	1,076	6,150	40,920
	WV-2	2/27/2014	13,999	688	129	46	1,606	16,468
	WV-3	2/13/2015	17,578	858	125	273	5,267	24,101
Low sun elev. & snow-free	WV-1	6/13/2013	58,886	6,368	2,422	2,306	17,432	87,414
	WV-1	6/17/2013	4,226	2,775	451	181	650	8,283
	WV-2	6/9/2015	10,695	2,131	1,224	1,512	6,070	21,632
	WV-2	7/11/2015	2,206	308	597	352	800	4,263
	WV-2	6/30/2016	926	200	40	30	232	1,428

The distributions of differences between DSM canopy surfaces and lidar reveal a few general patterns. Figure 3 shows these distributions as boxplots, grouped according to DSM type, arranged vertically by canopy surface (percentile height), and faceted by canopy cover. The boxplots show that the distributions in DSM canopy surfaces from reference LiDAR change with DSM type and with canopy cover. They also show that, generally, DSM forest surfaces underestimate the uppermost canopy surfaces (p90 - p100). Third, the DSM estimates from data acquired during periods with snow cover show the largest underestimates in moderate (40 - 60 %) and dense canopy cover (> 60%). In the TIU study area, reference lidar indicate broad differences in canopy height distributions between the uppermost canopy surfaces (p100) in dense relative to sparse (1 – 20 %) cover (reference median p100 heights are 17.9 m and 5.9 m, respectively). In the facet representing sparse cover, these aggregate distributions show little difference between estimates of canopy surfaces from the 4 DSM types. However, in the facets for dense cover, the "High sun elev. & snow" DSMs feature the broadest distributions that underestimate canopies, particularly for upper level canopy surfaces. These results show that where cover is most homogenous, the differences in how DSMs estimate canopy surfaces are most apparent, whereas in very sparse and likely more heterogeneous cover this study does not resolve such differences.

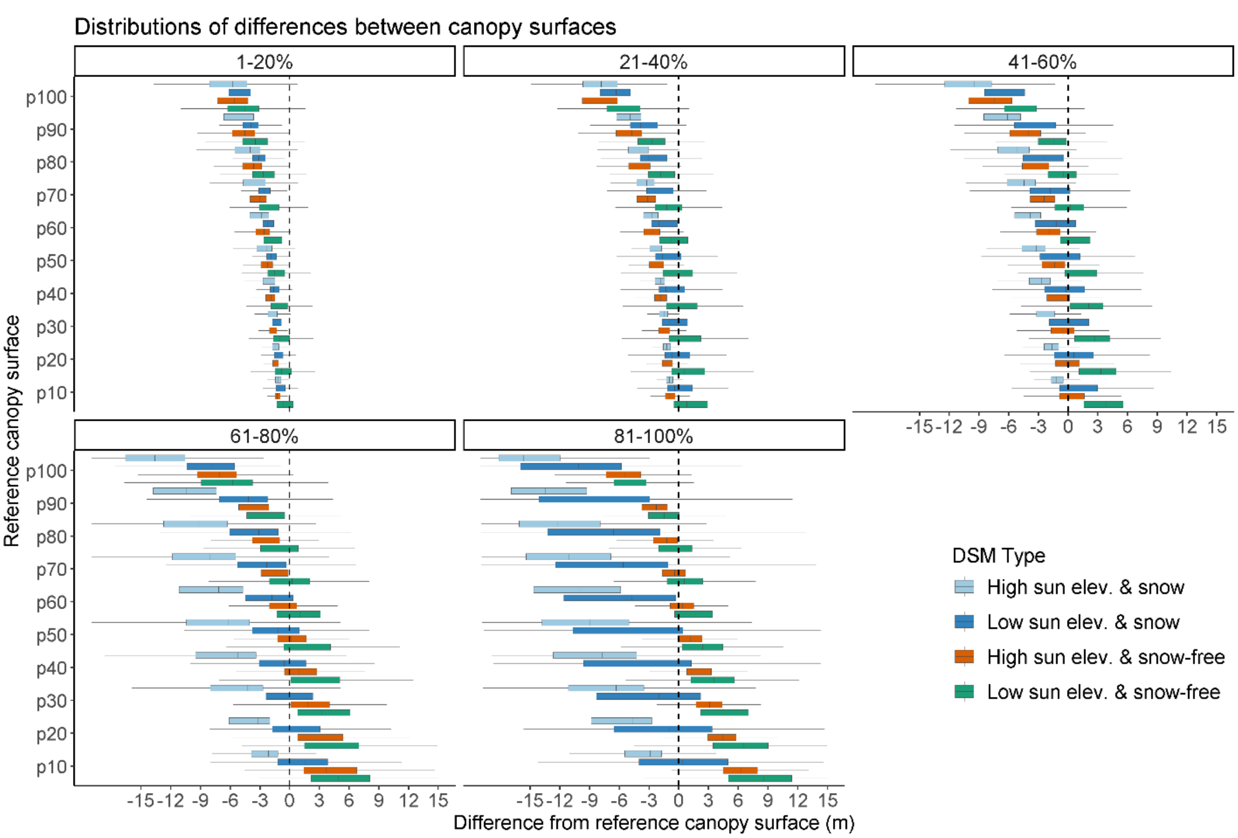

Figure 3. Boxplots show the distributions of differences between HRSI DSMs and reference canopy surfaces for each DSM type across 5 canopy cover intervals.

A summary of the central tendency and the variance of each distribution of differences provides insight into the approximate position in the vertical canopy column of the HRSI DSM canopy surface estimates. Figure 4 shows the median (left group) and the corresponding robust variance estimate expressed as the normalized median absolute difference (NMAD; right group) of each difference distribution for each percentile height within each 20% canopy cover interval (Höhle and Höhle 2009). The summary plots showing median values describe the similarity, or, the association of reference canopy surfaces with those DSM canopy surfaces across type and canopy cover interval. The corresponding NMAD plots convey the uncertainty associated with the median plots. Together, these summary plots demonstrate how the summary statistics change with cover, canopy percentile height surface, and DSM type.

Table 2 reports the representative canopy surfaces of HRSI DSMs. These surfaces are those reference canopy percentile height surfaces most similar to (that minimize the difference with) the canopy surfaces from HRSI DSMs. This table shows the 2 reference percentile heights that have the smallest and 2nd smallest absolute median difference to the HRSI DSM canopy surfaces for each DSM type and reference canopy cover interval. We note a few important observations about the representative canopy surfaces from HRSI DSMs from this minimization. The medians of these distributions show that, in general, "Low sun elev. & snow-free" DSM surfaces (Figure 4a, top left) in dense (> 60% cover) and moderate (40 – 60% cover) canopies are most representative of reference p70 - p80 surfaces. The "High sun elev. & snow-free" DSM surfaces (Figure 4a, top right) in dense canopies are most representative of surfaces p50 – p70. The canopy surfaces from DSM types with snow are most representative of percentile height surfaces representing lower canopy surface (p10 – p40) across all cover intervals.

The NMADs of the difference distributions provide some context for understanding and weighting the estimates of representative surfaces. In dense canopy cover (> 60%), where DSMs with snow most significantly underestimate canopy surfaces, NMADs are largest. Those of near-ground canopy surfaces (p10) are, on average, lowest for canopy cover < 40% from “High sun elev.” DSMs (snow and snow-free). The NMADs of the most representative surface (p60) from the DSMs of type “High sun elev. & snow-free” in the most dense cover interval is particularly large (6.68 m), whereas that of the 2nd most representative surface (p70) has a significantly smaller NMAD (1.34 m).

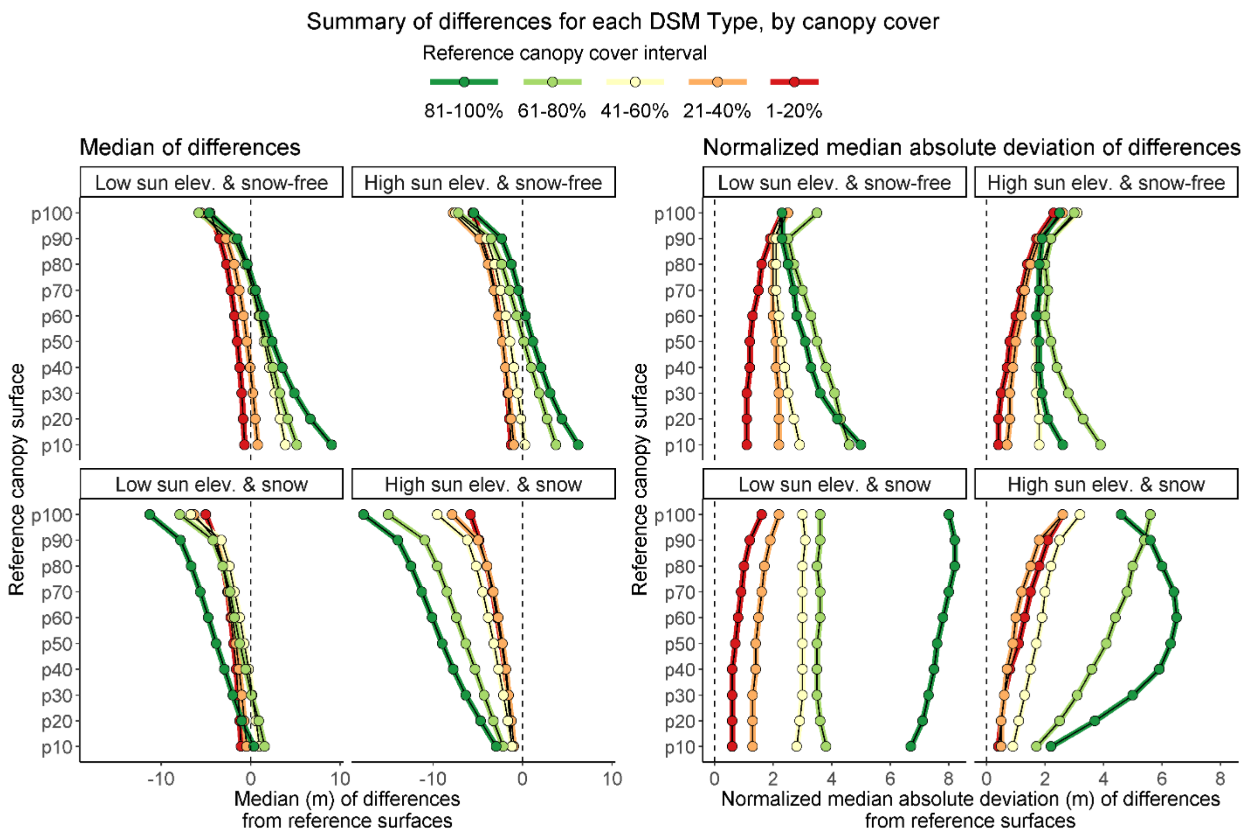

Figure 4. The summary of distributions of differences between aggregated DSM canopy surface estimates and those from reference lidar. Median (left group) and normalized median absolute deviation (right group) of DSM differences from reference percentile height surfaces across each reference canopy cover interval for 4 DSM types.

Table 2. Representative canopy surfaces of HRSI DSMs. These surfaces are those 2 reference percentile heights that have the smallest absolute median difference to the HRSI DSM canopy surfaces for each DSM type and reference canopy cover interval.

DSM type	Reference canopy cover	Representative canopy surfaces of HRSI DSMs					
		Most similar (1st minimum)			Second most similar (2nd minimum)		
		Name	Median difference (m)	NMAD of difference (m)	Name	Median difference (m)	NMAD of difference (m)
High sun elev. & snow	1-20%	p10	-1.19	0.41	p20	0.25	1.8
	21-40%	p10	-0.95	0.49	p20	-1.42	0.5
	41-60%	p10	-1.17	0.86	p20	-1.23	0.53
	61-80%	p10	-2.16	1.72	p20	-1.64	1.07
	81-100%	p10	-2.93	2.25	p20	-3.25	2.47
High sun elev. & snow-free	1-20%	p10	-1.28	0.36	p20	-4.69	3.68
	21-40%	p10	-0.99	0.7	p20	-1.47	0.44
	41-60%	p20	-1.06	0.56	p10	-1.27	0.75
	61-80%	p50	-0.44	1.34	p60	-1.24	0.56
	81-100%	p60	0.34	6.68	p70	-0.72	1.34
Low sun elev. & snow	1-20%	p10	-0.67	1.09	p20	-0.98	7.09
	21-40%	p10	-0.14	1.77	p20	-0.83	1.09
	41-60%	p30	0.16	2.98	p40	0.24	2.16
	61-80%	p30	0.09	3.48	p40	-0.23	2.97
	81-100%	p10	-0.07	2.1	p20	-0.58	3.52
Low sun elev. & snow-free	1-20%	p10	0.15	2.17	p20	-0.63	2.04
	21-40%	p40	0.36	1.74	p30	-0.42	1.75
	41-60%	p70	0.24	2.13	p80	0.54	2.67
	61-80%	p70	0.24	2.97	p80	-0.5	2.1
	81-100%	p80	-0.39	2.49	p70	-0.61	2.7

Figure 5 summarizes the proportions of representative canopy surfaces for each type of HRSI DSMs, showing (1) how representative these surfaces are of the various reference percentile heights, and (2) the pattern of representative canopy surfaces across cover intervals. The top row of the figure shows the distribution of the minimized differences of all the representative surfaces compiled for the set of DSMs in this study. Most minimized differences are < 1 m from the closest reference percentlie height canopy surface in TIU forests. The primary differences in the distributions from each type of DSM are in both the shape of the distributions associated with p10 surfaces (the closest canopy surface to the ground) and in the relative proportion of each canopy surface that accounts for the minimized difference (the most similar surface). When the p10 surfaces are most representative of canopy surfaces from HRSI DSMs, they are so with the greatest differences from them.

The middle and bottom rows show the pattern of representative canopy surfaces across reference and Landsat canopy cover intervals, and the extent to which canopy cover influences DSM estimates of canopy surfaces. The proportion of canopy surfaces that are most similar to surfaces from HRSI DSMs vary with canopy cover, and this variation differs with DSM type. Here, for each DSM type, the proportions of the reference canopy percentile height surfaces are shown for each 10 % bin of reference canopy cover. Under the same ground conditions, the differences in per-bin proportional contributions are particularly apparent between the 2 'snow-free' types of DSMs in sparse (canopy cover 1 -20 %) and open canopy (canopy cover 21 - 40 %) forests. Between these two types of DSMs in sparse and open canopies, reference surfaces from the upper canopy (p60 - p100) account for very different proportions of the total set of reference surfaces most similar to those from the DSMs. These upper-canopy surfaces account for 2 % of the total for "High sun elev. & snow-free" DSMs, while accounting for 29 % of the total for "Low sun elev. & snow-free" DSMs. The proportions of these upper-canopy surfaces between these two types of snow-free DSMs begin to look more similar > 60 % canopy cover (46 % and 63 %, respectively, for "High sun elev. & snow-free" and "Low sun elev. & snow-free" DSMs). Thus, as canopy cover decreases, the estimates of canopy surfaces from DSMs acquired under different sun elevations increasingly diverge.

Ground surface condition is also linked to divergent DSM estimates of canopy surfaces. Large differences in these proportions appear between snow and snow-free DSMs. Of those DSMs with snow, those of type "High sun elev. & snow" have proportionally very few surfaces that are closely associated with the upper canopy in both sparse and open canopies (1 %) and dense canopies (2 %). Furthermore, across all canopy cover for DSMs with snow, 94 % ("High sun elev. & snow") and 78 % ("Low sun elev. & snow") of the DSM canopy surfaces are most similar to that which is nearest to ground (p10). In this study, when snow covered the ground in the images used to generate HRSI DSMs, upper-canopy surfaces were less frequently captured, particularly in sparse and open canopies.

Spaceborne estimates of canopy cover from Landsat reveal similar patterns of divergence between canopy surface estimates of the various DSM types. Figure 5 (bottom row) shows the proportion of reference canopy surfaces most similar to those from HRSI DSMs for tree cover intervals derived from Landsat, where estimates of cover were calibrated to account for tree canopies greater than 2 m tall (Montesano et al., 2016). The proportions in tree cover intervals > 70 % cover were based on very few observations (n < 30), and thus excluded from the figure.

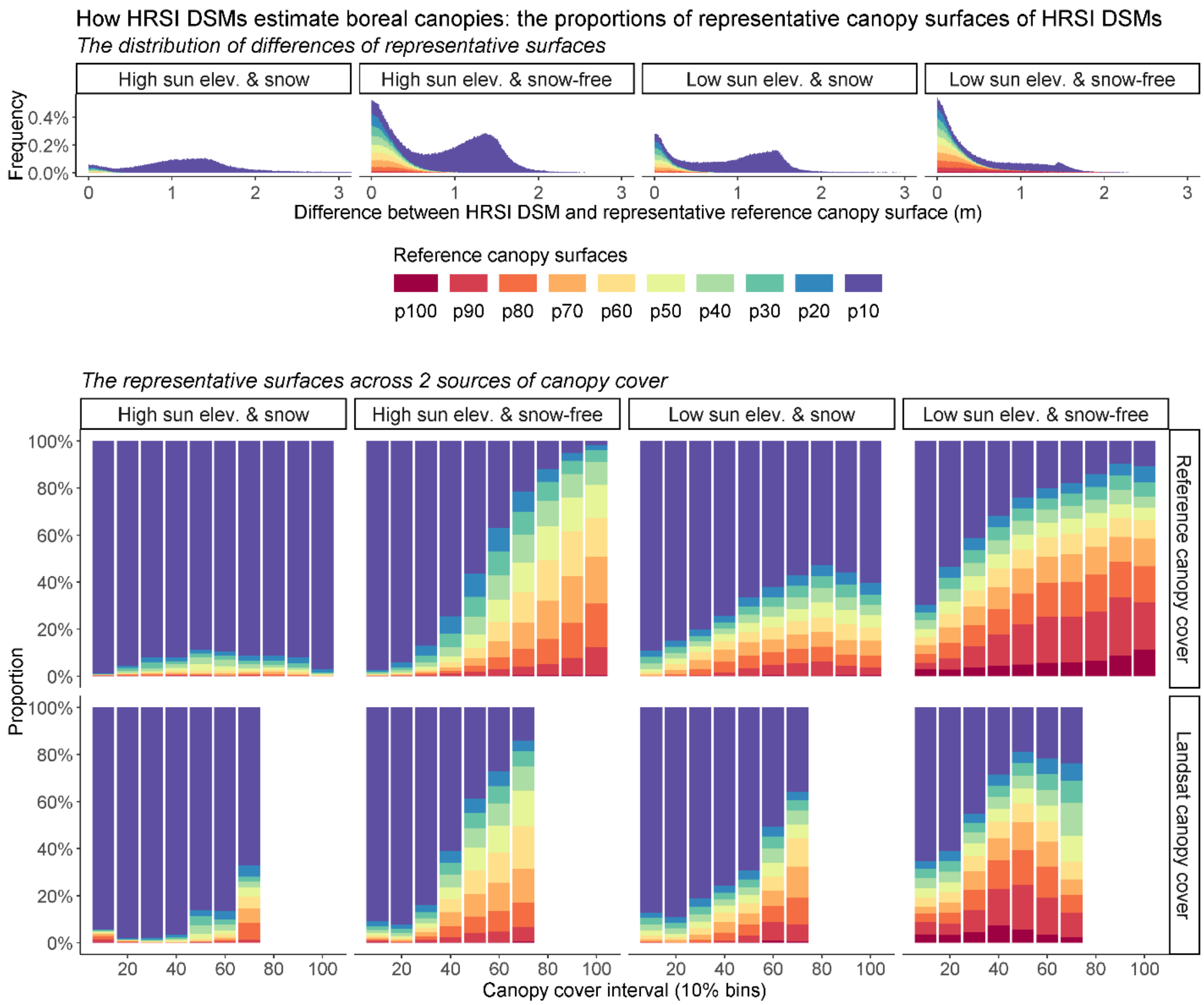

Figure 5. Representative canopy surfaces of HRSI DSMs in the TIU boreal study domain. (Top row) The distribution of the differences between HRSI DSM boreal forest canopy surfaces and reference for all representative surfaces. (Middle and bottom row) The relative proportions of representative canopy surfaces across canopy cover intervals from (a) reference canopy and (b) calibrated Landsat canopy cover

(Montesano et al., 2016). Note: Landsat tree canopy cover bins > 70 % each had fewer than 30 observations.

The 3 example sites in Figure 6 highlight the spatial variation in the representative canopy surfaces of HRSI DSMs. In this example, a reference canopy cover map provides context for the canopy surfaces (percentile heights) maps that are most representative of DSM canopy surface estimates at 3 different sites (rows in the figure). Site 1 features a case where dense cover is represented primarily with a 10^{th} percentile height surface, and less dense cover with upper canopy surfaces, from a DSM of type "Low sun elev. & snow" while the corresponding snow-free results show generally the inverse. The center panel "Low sun elev. & snow" example at this site demonstrates how the combined effects of variable light conditions, snow, and topography (not shown) can make for particularly difficult interpretation of canopy surface estimates. Site 2 features more variable forest cover where the "Low sun elev. & snow-free" DSM captures upper canopy surfaces in dense and moderate cover where the "High sun elev. & snow" DSM does not. Site 3 shows canopy surfaces from a DSM of type "High sun elev. & snow" DSM along with one of type "High sun elev. & snow-free". In particular, this site illustrates the differences in the canopy surfaces that are captured by these two different DSMs in areas of dense forest cover, where the DSM with snow present features surface estimates most similar to the 10th percentile height surface. These examples at these sites do not show where patterns of representative surfaces may be affected by topographic effects such as local viewing and solar geometry.

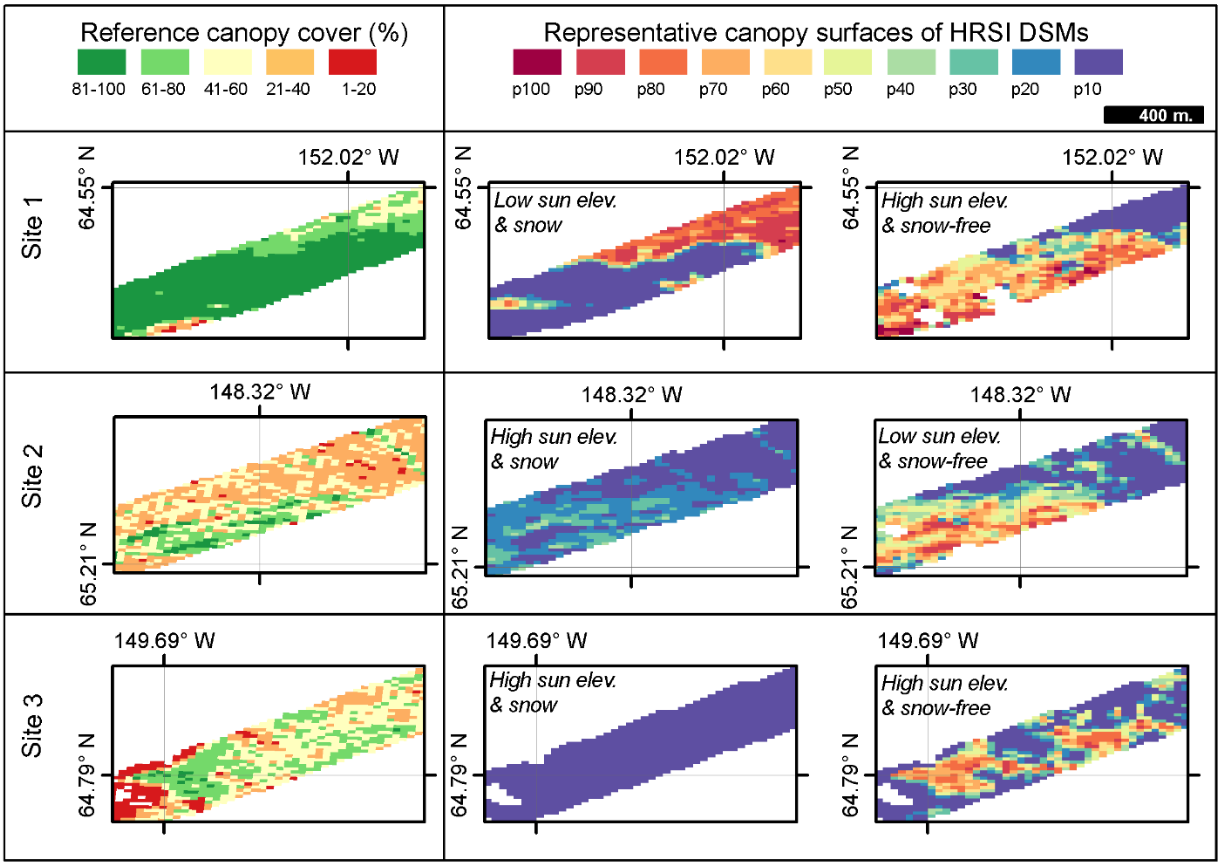

Figure 6. Examples of representative canopy surfaces of HRSI DSMs at 3 sites in the study area show how the variations in both canopy cover and DSM type are associated with variations in the boreal canopy surfaces they capture. For each site, the reference canopy cover (left column) is shown for the corresponding representative surfaces from 2 DSM types: with snow (middle column) and snow-free (right column).

Discussion

These results demonstrate the significant variation in boreal canopy surfaces that exists among HRSI DSMs. These data provide insight into which boreal forest canopy surfaces are captured in 4 general types of DSMs derived from automated stereogrammetry available in the archive of DigitalGlobe along-track stereopairs. We show that there is variability in the types of vertical canopy surfaces estimated from DSMs and that this variability has a temporal and spatial component. Temporally, the variability depends on the type of DSM described by an acquisition's solar information (solar elevation angle) and seasonality, which may include ground condition and vegetation phenology. The spatial variability is associated with the density of the forest canopy cover. Altogether, the DSM difference estimates and the representative surfaces provide a general understanding of the canopies that are captured with the variety of DSMs in this study, and which represent significant cohorts of data available in the broader DigitalGlobe archive.

Boreal canopy surfaces from HRSI DSMs

For boreal canopy surfaces from HRSI DSMs, the results show that in the Tanana Valley (1) DSMs grouped by sun elevation angle and the presence of snow provide different surface estimates for boreal canopies, (2) the two DSM types that appear to most differently capture boreal forest canopy surfaces are the type "Low sun elev. & snow-free" and "High sun elev. & snow", (3) that DSMs with snow less frequently capture upper canopy surfaces, (4) the "Low sun elev. & snow-free" DSMs provide surfaces, on average, that are most similar to upper-canopy surfaces (dense forests > 60% cover, 70th - 80th percentile heights), and (5) in the most dense forests (> 80% cover) where canopy gaps are least likely to bias downward the average surface estimates from the 13 m pixels, the snow-free DSM types are most closely associated with 70th - 80th percentile heights ("Low sun elev. & snow-free") and 60th - 70th percentile heights ("High sun elev. & snow-free"). These results can be used to guide the acquisition and application of HRSI DSMs and their estimates for characterizing boreal forest structure, and to inform the interpretation of boreal forest surfaces from these data and their derived products.

In this study, snow-free DSMs provided the best representation of upper-canopy surfaces. These DSM canopy surface estimates range from 60th - 80th percentile heights and this range among snow-free DSMs from low and high sun elevation acquisitions is difficult to fully explain with this analysis. Differences in the shadowing or occlusion of canopy gaps may account for the differences in the percentile heights that are most closely associated with the DSMs' respective canopy surfaces. The 13 m resolution of the reference data determined the DSM resolution of analysis, and the extent to which pixels mixed their surface estimates from upper and lower canopies. In the most dense canopies, DSM estimates are less likely to come from lower in the canopies, so the estimates in dense canopies (where cover is often nearly continuous at the resolution of this analysis) may provide the clearest explanation of which vertical portion of the canopy surface distribution accounts for the canopy surfaces that are captured when 100% of a given pixel is forest canopy, irrespective of pixel size.

Features of seasonality, geometry as a source of uncertainty

These results are most applicable for boreal forests in high latitude regions where acquisitions cover a range of sun elevation angles, underneath a range of forest canopies, with conditions that differ based on features of seasonality and local viewing and solar geometry. These features may contribute to the overall uncertainty of the estimates of forest canopy surfaces, and, in particular may account for some of the DSM underestimation.

In this study, we identify the presence of snow as determining a general type of DSM. This is because snow influences the local contrast between features of interest (i.e., trees) and the ground. The presence of snow is one component of seasonality of the image scene, the full scope of which is not entirely handled in this analysis. The presence of snow in an image scene may have at least 2 effects. First, it may affect the co-registration between ground control surfaces where the depth of the snow raises the ground surface relative to the canopy, resulting in greater underestimation of canopy surfaces. Indeed, our results show greater underestimation of canopy surfaces from DSMs with snow. Second, it implies the leaf-off state of deciduous vegetation, which is a prominent portion of the forest patches across the TIU. It is noteworthy that DSM types with snow may poorly represent forest canopy surfaces not only because of the reduced contrast of well-illuminated forest surfaces with bright snow, but also because of the reduced ability of images to resolve deciduous forest surfaces without their leaves. Furthermore, DSMs without snow may still underestimate deciduous canopy surfaces if data were acquired before leaves have fully emerged. We note that further dividing forest canopy cover into deciduous and coniferous types, and better constraining acquisitions based on vegetation phonology, could improve understanding of DSM underestimates.

Our results do not fully address the geometric component of DSM canopy surface variation. This study's general grouping of DSMs according to solar geometry does not enable a detailed understanding of how the geometry of local solar and viewing angles influence canopy surface estimates from automated stereogrammetry. There is likely significant local sun elevation angle effects that mix contributions from terrain aspect, slope, and viewing geometry to the overall uncertainty of these estimates. Ultimately, geometric-optical radiative transfer modelling of simulated canopy surfaces of varying densities may provide the clearest accounting of the relative weights of these acquisition characteristics on canopy surface estimates (Yin et al., 2015). Stereogrammetry applied to these simulated surfaces will likely provide a means of producing canopy surface bias corrections that are forest pattern or image texture specific, and can then be applied in a geographic weighting scheme to provide spatially explicit forest structure corrections to address variations in canopy surface estimates from different local geometry.

Canopy surface estimates in low canopy cover

In low canopy cover (< 40%), where trees can either be arranged sparsely or in infrequent small, dense clusters, these aggregate distributions do not resolve differences in estimates of canopy surfaces from the 4 DSM types. This lack of resolution is one potential source of the underestimation of canopy surfaces in low canopy cover, and agree with other recent stereo-derived canopy surface results (Ni et al., 2018). Underestimates in this portion of domain may account for the increased proportion of the p10 surface being the most representative of surfaces provided by the DSMs. The distributions of these p10 underestimates show peaks between 1 - 2 m for the subset of the domain < 40% canopy cover for which reference data indicate a median p100 canopy surface height of ~ 6 m. We know from previous work (Montesano et al. 2017) that DSMs from images acquired at low sun elevation angles reveal upper canopy surfaces at fine scales. However, the 13 m resolution of this analysis was not designed to resolve the detailed patterns of canopy in sparse and heterogeneous cover conditions, where there is likely significant sup-pixel heterogeneity in forest structure. This trade-off in horizontal spatial resolution was made in order to have sufficient vertical resolution. The 10 canopy percentile height surfaces provided important insight into which portion of the vertical column of canopy surfaces are most representative of surfaces in the 4 types of DSMs where cover is generally homogenous.

Informing the use of boreal forest surface estimates from HRSI DSMs

It is important to recognize differences in DSM estimates of boreal canopies in order to accurately interpret the direct estimates of canopy surfaces and model forest structure characteristics. Our results suggest that forest cover, in part, determines which vertical canopy surfaces in boreal forests are resolved. Forest cover is associated with the likelihood that forest surfaces from HRSI DSMs describe the upper portions of boreal forest canopies. At our study sites, the denser the forest cover, the more likely that HRSI DSMs estimates described canopy surfaces at the higher end of surfaces within the 60th - 80th percentile heights range. Therefore, prior knowledge of forest cover may provide a means for anticipating which canopy surfaces are representative of DSM surfaces in forested areas. This could be a useful component of a multi-scale, multi-sensor geostatistical framework for estimating carbon stocks outside of forest structure estimates from either high fidelity swaths of airborne lidar or lidar footprint samples. In fact, using prior forest cover estimates to understand HRSI DSM-derived height canopy surfaces would extend the "Landsat-as-prior" methodology that are already part of such frameworks (Babcock et al., 2018).

Ultimately, standardizing the canopy surface estimation from these DSMs will simplify the interpretation of, and the modelling with, these DSM canopy surfaces. This can be done by either constraining the range of acquisitions, selecting only for certain acquisitions that will provide canopy estimates that can be well understood, or correcting for the differences in estimates that arise with different canopy cover and sun-sensor-target geometry. Without this prior understanding of these forest structure and acquisition details, models that use forest structure estimates from these DSMs could yield more uncertain results.

Informing the interpretation of forests from the ArcticDEM

The results show that different types of DSMs provide estimates of different canopy surfaces where forest canopy is present. This is important to recognize in light of the availability of the ArcticDEM, its potential for forest structure characterization across Arctic and sub-arctic forests, and the variety of DSMs that have been used to generate this pan-Arctic product. Our results suggest that the forest canopy signal that is embedded in this product will likely be spatially inconsistent, and this inconsistency is driven in part by the differences in how automated stereogrammetry routines estimate surface elevations from DigitalGlobe data of forest canopies when their surfaces, illumination conditions, and their ground conditions vary. This inconsistency in the product's interpretation of forest surfaces will have implications for the broad-scale interpretation of consistent forest structure characteristics. These forests feature a wide range of important structural characteristics in terms of density, height and spatial pattern, and their interpretation will vary depending on the individual of group of DSMs used to compile the surface estimate coincident with the forest canopies. Since these HRSI DSM data and derived products offer some of the first glimpses of fine-scaled structural patterns across broad and remote Arctic forests, they can provide new opportunities for understanding the spatial distribution of forest dynamics if we can account for how these forest surface estimates will vary, and control that variation to improve the consistency of forest surface estimates across the boreal domain.

Conclusions

We explored the variation of HRSI DSM estimates of boreal canopy surfaces by comparing the distributions of differences in boreal canopy percentile heights derived from reference small footprint lidar in Tanana Valley, Alaska with surface elevations derived from these 4 types of HRSI DSMs. We examined the relationship in the variability of canopy surface estimates from HRSI DSMs to acquisition information and canopy cover. Our results help clarify which boreal canopy surfaces are representative of those captured with HRSI DSMs. They show that in the Tanana Valley (1) DSMs grouped by sun elevation angle and the presence of snow provide different surface estimates for boreal canopies in dense cover; (2) the two DSM types that appear to most differently capture boreal forest canopy surfaces are DSMs from snow-free images acquired at sun elevation angles < 30 ("Low sun elev. & snow-free") and those with snow-cover at sun elevation angles > 30 ("High sun elev. & snow-free"); (3) DSMs with snow most often do not capture upper canopy surfaces; (4) the "Low sun elev. & snow-free" DSMs provide surfaces, on average, that are most representative of upper canopy surfaces (dense forests > 60% cover, 70th - 80th percentile heights); and (5) in the most dense forests (> 80% cover) where canopy gaps are least likely to bias downward the average surface estimates, snow-free DSM types are most representative of 70^{th} - 80th percentile heights ("Low sun elev. & snow-free") and 60th - 70th percentile heights ("High sun elev. & snow-free"). The combination of horizontal forest structure and acquisition characteristics affect the vertical structure estimates of boreal canopy surface from spaceborne stereogrammetry. These affects should be considered when analyzing forest structure derived from HRSI DSMs, and as part of a comprehensive approach to spaceborne remote sensing of circumpolar boreal forests.

Acknowledgements

This work was supported by both formal and informal collaborations with the following people and groups: Dan Duffy, Scott Sinno, Hoot Thompson and the ADAPT team at NASA GSFC for high-performance computing support; Anika Halota for GLiHT data discovery and access tools; David Shean for open-source code repositories for HRSI DEM processing; the Polar Geospatial Center under NSF-OPP awards 1043681, 1559691, and 1542736 for ArcticDEMs. DigitalGlobe data were provided by NASA's NGA Commercial Archive Data (cad4nasa.gsfc.nasa.gov) under the National Geospatial-Intelligence Agency's NextView license agreement.

References

Alexander, H.D., Mack, M.C., Goetz, S., Loranty, M.M., Beck, P.S.A., Earl, K., Zimov, S., Davydov, S., Thompson, C.C., 2012. Carbon Accumulation Patterns During Post-Fire Succession in Cajander Larch (Larix cajanderi) Forests of Siberia. Ecosystems 15, 1065–1082.

Babcock, C., Finley, A.O., Andersen, H.-E., Pattison, R., Cook, B.D., Morton, D.C., Alonzo, M., Nelson, R., Gregoire, T., Ene, L., Gobakken, T., Næsset, E., 2018. Geostatistical estimation of forest biomass in interior Alaska combining Landsat-derived tree cover, sampled airborne lidar and field observations. Remote Sens. Environ. 212, 212–230.

Babcock, C., Finley, A.O., Bradford, J.B., Kolka, R., Birdsey, R., Ryan, M.G., 2015. LiDAR based prediction of forest biomass using hierarchical models with spatially varying coefficients. Remote Sens. Environ. 169, 113–127.

Beguet, B., Chehata, N., Boukir, S., Guyon, D., 2014. Classification of forest structure using very high resolution Pleiades image texture, in: 2014 IEEE Geoscience and Remote Sensing Symposium. https://doi.org/10.1109/igarss.2014.6946936

Bohlin, J., Wallerman, J., Fransson, J.E.S., 2012. Forest variable estimation using photogrammetric matching of digital aerial images in combination with a high-resolution DEM. Scand. J. For. Res. 27, 692–699.

Cook, B., Corp, L., Nelson, R., Middleton, E., Morton, D., McCorkel, J., Masek, J., Ranson, K., Ly, V., Montesano, P., 2013. NASA Goddard's LiDAR, Hyperspectral and Thermal (G-LiHT) Airborne Imager. Remote Sensing 5, 4045–4066.

Corp, L.A., Cook, B.D., McCorkel, J., Middleton, E.M., 2015. Data products of NASA Goddard's LiDAR, hyperspectral, and thermal airborne imager (G-LiHT), in: Next-Generation Spectroscopic Technologies VIII. https://doi.org/10.1117/12.2177083

Dai, C., Durand, M., Howat, I.M., Altenau, E.H., Pavelsky, T.M., 2018. Estimating River Surface Elevation From ArcticDEM. Geophys. Res. Lett. 45, 3107–3114.

Dai, C., Howat, I.M., 2017. Measuring Lava Flows With ArcticDEM: Application to the 2012-2013 Eruption of Tolbachik, Kamchatka. Geophys. Res. Lett. 44, 12,133–12,140.

DigitalGlobe, 2014. Geolocation Accuracy of WorldView Products (White Paper).

Fassnacht, F.E., Mangold, D., Schäfer, J., Immitzer, M., Kattenborn, T., Koch, B., Latifi, H., 2017. Estimating stand density, biomass and tree species from very high resolution stereo-imagery – towards an all-in-one sensor for forestry applications? Forestry: An International Journal of Forest Research 90, 613–631.

Finley, A.O., Banerjee, S., Zhou, Y., Cook, B.D., Babcock, C., 2017. Joint hierarchical models for sparsely sampled high-dimensional LiDAR and forest variables. Remote Sens. Environ. 190, 149–161.

Forkel, M., Carvalhais, N., Rödenbeck, C., Keeling, R., Heimann, M., Thonicke, K., Zaehle, S., Reichstein, M., 2016. Enhanced seasonal CO2 exchange caused by amplified plant productivity in northern ecosystems. Science 351, 696–699.

Harper, K.A., Danby, R.K., De Fields, D.L., Lewis, K.P., Trant, A.J., Starzomski, B.M., Savidge, R., Hermanutz, L., 2011. Tree spatial pattern within the forest–tundra ecotone: a comparison of sites across CanadaThis article is a contribution to the series Tree recruitment, growth, and distribution at the circumpolar forest–tundra transition. Can. J. For. Res. 41, 479–489.

Hawryło, P., Tompalski, P., Wężyk, P., 2017. Area-based estimation of growing stock volume in Scots pine stands using ALS and airborne image-based point clouds. Forestry: An International Journal of Forest Research 90, 686–696.

Hobi, M.L., Ginzler, C., Commarmot, B., Bugmann, H., 2015. Gap pattern of the largest primeval beech forest of Europe revealed by remote sensing. Ecosphere 6, art76.

Höhle, J., Höhle, M., 2009. Accuracy assessment of digital elevation models by means of robust statistical methods. ISPRS J. Photogramm. Remote Sens. 64, 398–406.

Honkavaara, E., Markelin, L., Rosnell, T., Nurminen, K., 2012. Influence of solar elevation in radiometric and geometric performance of multispectral photogrammetry. ISPRS J. Photogramm. Remote Sens. 67, 13–26.

Hurtt, G.C., Thomas, R.Q., Fisk, J.P., Dubayah, R.O., Sheldon, S.L., 2016. The Impact of Fine-Scale

Disturbances on the Predictability of Vegetation Dynamics and Carbon Flux. PLoS One 11, e0152883.

Immitzer, M., Stepper, C., Böck, S., Straub, C., Atzberger, C., 2016. Use of WorldView-2 stereo imagery and National Forest Inventory data for wall-to-wall mapping of growing stock. For. Ecol. Manage. 359, 232–246.

Järnstedt, J., Pekkarinen, A., Tuominen, S., Ginzler, C., Holopainen, M., Viitala, R., 2012. Forest variable estimation using a high-resolution digital surface model. ISPRS J. Photogramm. Remote Sens. 74, 78–84.

Kattenborn, T., Maack, J., Faßnacht, F., Enßle, F., Ermert, J., Koch, B., 2015. Mapping forest biomass from space – Fusion of hyperspectral EO1-hyperion data and Tandem-X and WorldView-2 canopy height models. Int. J. Appl. Earth Obs. Geoinf. 35, 359–367.

Meddens, A.J.H., Vierling, L.A., Eitel, J.U.H., Jennewein, J.S., White, J.C., Wulder, M.A., 2018. Developing 5 m resolution canopy height and digital terrain models from WorldView and ArcticDEM data. Remote Sens. Environ. 218, 174–188.

Montesano, P.M., Neigh, C., Sun, G., Duncanson, L., Van Den Hoek, J., Jon Ranson, K., 2017. The use of sun elevation angle for stereogrammetric boreal forest height in open canopies. Remote Sens. Environ. 196, 76–88.

Montesano, P., Neigh, C., Sexton, J., Feng, M., Channan, S., Ranson, K., Townshend, J., 2016. Calibration and Validation of Landsat Tree Cover in the Taiga−Tundra Ecotone. Remote Sensing 8, 551.

Morin, P., Porter, C., Cloutier, M., Howat, I., Noh, M. J., Willis, M., et al. (2016). ArcticDEM; a publically available, high resolution elevation model of the Arctic. EGU General Assembly Conference Abstracts, 18, 8396.

Moskal, L.M., Franklin, S.E., 2002. Multi-layer Forest Stand Discrimination with Spatial Co-occurrence Texture Analysis of High Spatial Detail Airborne Imagery. Geocarto Int. 17, 55–68.

Neigh, C., Masek, J., Bourget, P., Cook, B., Huang, C., Rishmawi, K., Zhao, F., 2014. Deciphering the

Precision of Stereo IKONOS Canopy Height Models for US Forests with G-LiHT Airborne LiDAR. Remote Sensing 6, 1762–1782.

Neigh, C.S.R., Masek, J.G., Nickeson, J.E., 2013. High-Resolution Satellite Data Open for Government Research. Eos Trans. Amer. Geophys. Union 94, 121–123.

Ni, W., Sun, G., Pang, Y., Zhang, Z., Liu, J., Yang, A., Wang, Y., Zhang, D., 2018. Mapping Three-Dimensional Structures of Forest Canopy Using UAV Stereo Imagery: Evaluating Impacts of Forward Overlaps and Image Resolutions With LiDAR Data as Reference. IEEE Journal of Selected Topics in Applied Earth Observations and Remote Sensing, 11, 1–12.

Noh, M.-J., Howat, I.M., 2017. The Surface Extraction from TIN based Search-space Minimization (SETSM) algorithm. ISPRS J. Photogramm. Remote Sens. 129, 55–76.

Noh, M.-J., Howat, I.M., 2015. Automated stereo-photogrammetric DEM generation at high latitudes: Surface Extraction with TIN-based Search-space Minimization (SETSM) validation and demonstration over glaciated regions. GISci. Remote Sens. 52, 198–217.

Pan, Y., Birdsey, R.A., Fang, J., Houghton, R., Kauppi, P.E., Kurz, W.A., Phillips, O.L., Shvidenko, A., Lewis, S.L., Canadell, J.G., Ciais, P., Jackson, R.B., Pacala, S.W., McGuire, A.D., Piao, S., Rautiainen, A., Sitch, S., Hayes, D., 2011. A large and persistent carbon sink in the world's forests. Science 333, 988–993.

Persson, H.J., Perko, R., 2016. Assessment of boreal forest height from WorldView-2 satellite stereo images. Remote Sens. Lett. 7, 1150–1159.

Porter, C., Morin, P., Howat, I., Noh, M.J., Bates, B., Peterman, K., Keesey, S., Schlenk, M., Gardiner, J., Tomko, K., Willis, M., Cloutier, M., Husby, E., Foga, S., Nakamura, H., Platson, M., Wethington Jr., M., Williamson, C., Bauer, G., Enos, J., Arnold, G., Kramer, W., Becker, P., Doshi, A., D'Souza, C., Cummens, P., Laurier, F., Bojesen, M. 2018. "ArcticDEM" https://doi.org/10.7910/DVN/OHHUKH, Harvard Dataverse, V1

Puliti, S., Gobakken, T., Ørka, H.O., Næsset, E., 2016. Assessing 3D point clouds from aerial photographs for species-specific forest inventories. Scand. J. For. Res. 32, 68–79.

Puliti, S., Saarela, S., Gobakken, T., Ståhl, G., Næsset, E., 2018. Combining UAV and Sentinel-2 auxiliary data for forest growing stock volume estimation through hierarchical model-based inference. Remote Sens. Environ. 204, 485–497.

Saarela, S., Holm, S., Grafström, A., Schnell, S., Næsset, E., Gregoire, T.G., Nelson, R.F., Ståhl, G., 2016. Hierarchical model-based inference for forest inventory utilizing three sources of information. Ann. For. Sci. 73, 895–910.

Shean, D.E., Alexandrov, O., Moratto, Z.M., Smith, B.E., Joughin, I.R., Porter, C., Morin, P., 2016. An automated, open-source pipeline for mass production of digital elevation models (DEMs) from very-high-resolution commercial stereo satellite imagery. ISPRS J. Photogramm. Remote Sens. 116, 101–117.

Shugart, H.H., Saatchi, S., Hall, F.G., 2010. Importance of structure and its measurement in quantifying function of forest ecosystems. Journal of Geophysical Research: Biogeosciences 115. https://doi.org/10.1029/2009jg000993

Siewert, M.B., Hanisch, J., Weiss, N., Kuhry, P., Maximov, T.C., Hugelius, G., 2015. Comparing carbon storage of Siberian tundra and taiga permafrost ecosystems at very high spatial resolution. Journal of Geophysical Research: Biogeosciences 120, 1973–1994.

Snyder, P.K., Liess, S., 2013. The simulated atmospheric response to expansion of the Arctic boreal forest biome. Clim. Dyn. 42, 487–503.

St-Onge, B., Hu, Y., Vega, C., 2008. Mapping the height and above-ground biomass of a mixed forest using lidar and stereo Ikonos images. Int. J. Remote Sens. 29, 1277–1294.

Straub, C., Tian, J., Seitz, R., Reinartz, P., 2013. Assessment of Cartosat-1 and WorldView-2 stereo imagery in combination with a LiDAR-DTM for timber volume estimation in a highly structured forest in Germany. Forestry 86, 463–473.

Stuart Chapin, F., Oswood, M.W., van Cleve, K., Viereck, L.A., Verbyla, D.L., 2006. Alaska's Changing Boreal Forest. Oxford University Press.

Vastaranta, M., Niemi, M., Karjalainen, M., Peuhkurinen, J., Kankare, V., Hyyppä, J., Holopainen, M.,

2014. Prediction of Forest Stand Attributes Using TerraSAR-X Stereo Imagery. Remote Sensing 6, 3227–3246.

Wang, L., Cole, J.N.S., Bartlett, P., Verseghy, D., Derksen, C., Brown, R., von Salzen, K., 2016. Investigating the spread in surface albedo for snow-covered forests in CMIP5 models. J. Geophys. Res. D: Atmos. 121, 1104–1119.

Webb, E.E., Heard, K., Natali, S.M., Bunn, A.G., Alexander, H.D., Berner, L.T., Kholodov, A., Loranty, M.M., Schade, J.D., Spektor, V., Zimov, N., 2017. Variability in above- and belowground carbon stocks in a Siberian larch watershed. Biogeosciences 14, 4279–4294.

White, J.C., Tompalski, P., Coops, N.C., Wulder, M.A., 2018. Comparison of airborne laser scanning and digital stereo imagery for characterizing forest canopy gaps in coastal temperate rainforests. Remote Sens. Environ. 208, 1–14.

Wulder, M.A., Ortlepp, S.M., White, J.C., Coops, N.C., 2008. Impact of sun-surface-sensor geometry upon multitemporal high spatial resolution satellite imagery. Can. J. Remote Sens. 34, 455–461.

Yin, T., Lauret, N., Gastellu-Etchegorry, J.-P., 2015. Simulating images of passive sensors with finite field of view by coupling 3-D radiative transfer model and sensor perspective projection. Remote Sens. Environ. 162, 169–185.

Captions for Figures

Figure 1. (a) Study sites in the Tanana Valley, Alaska where reference lidar provided reference measurements of horizontal and vertical forest structure for coincident strips of HRSI DSMs. (b) Aerial images of acquired during the 2014 airborne survey of the TIU with a digital single-lens reflex camera highlight a variety of forest structure patterns including (from left to right) small groups of conifers, dense continuous canopy, dense canopy adjacent to standing dead and fallen trees, and heterogeneous canopy cover.

Figure 2. Forest structure across the TIU study domain from reference lidar. The distributions of all reference canopy surface heights for 4 of the 10 percentile heights colored by canopy cover interval across the TIU study domain. Dashed lines and values in colored boxes show the median height values in meters for the corresponding canopy cover intervals.

Figure 3. Boxplots show the distributions of differences between HRSI DSMs and reference canopy surfaces for each DSM type across 5 canopy cover intervals.

Figure 4. The summary of distributions of differences between aggregated DSM canopy surface estimates and those from reference lidar. Median (left group) and normalized median absolute deviation (right group) of DSM differences from reference percentile height surfaces across each reference canopy cover interval for 4 DSM types.

Figure 5. Representative canopy surfaces of HRSI DSMs in the TIU boreal study domain. (Top row) The distribution of the differences between HRSI DSM boreal forest canopy surfaces and reference for all representative surfaces. (Middle and bottom row) The relative proportions of representative canopy surfaces across canopy cover intervals from (a) reference canopy and (b) calibrated Landsat canopy cover (Montesano et al., 2016). Note: Landsat tree canopy cover bins > 70 % each had fewer than 30 observations.

Figure 6. Examples of representative canopy surfaces of HRSI DSMs at 3 sites in the study area show how the variations in both canopy cover and DSM type are associated with variations in the boreal canopy surfaces they capture. For each site, the reference canopy cover (left column) is shown for the corresponding representative surfaces from 2 DSM types: with snow (middle column) and snow-free (right column).

793